Molecular Therapy
Nucleic Acids
Original Article

Hydrogel-Assisted Antisense LNA Gapmer Delivery for *In Situ* Gene Silencing in Spinal Cord Injury

Pedro M.D. Moreno,[1,2] Ana R. Ferreira,[1,2,9] Daniela Salvador,[1,2,9,10] Maria T. Rodrigues,[1,2] Marília Torrado,[1,2] Eva D. Carvalho,[1,2] Ulf Tedebark,[4,5] Mónica M. Sousa,[1,3] Isabel F. Amaral,[1,2] Jesper Wengel,[6] and Ana P. Pêgo[1,2,7,8]

[1]i3S - Instituto de Investigação e Inovação em Saúde, Universidade do Porto, 4200-135 Porto, Portugal; [2]INEB - Instituto de Engenharia Biomédica, Universidade do Porto, 4200-135 Porto, Portugal; [3]IBMC - Instituto de Biologia Molecular e Celular, Nerve Regeneration Group, Universidade do Porto, 4200-135 Porto, Portugal; [4]GE Healthcare Bio-Sciences AB, 75184 Uppsala, Sweden; [5]SynMer AB, 17568 Järfälla, Sweden; [6]Nucleic Acid Center, Department of Physics, Chemistry and Pharmacy, University of Southern Denmark, 5230 Odense, Denmark; [7]Faculdade de Engenharia da Universidade do Porto, 4200-465 Porto, Portugal; [8]Instituto de Ciências Biomédicas Abel Salazar (ICBAS), Universidade do Porto, 4050-313 Porto, Portugal

After spinal cord injury (SCI), nerve regeneration is severely hampered due to the establishment of a highly inhibitory microenvironment at the injury site, through the contribution of multiple factors. The potential of antisense oligonucleotides (AONs) to modify gene expression at different levels, allowing the regulation of cell survival and cell function, together with the availability of chemically modified nucleic acids with favorable biopharmaceutical properties, make AONs an attractive tool for novel SCI therapy developments. In this work, we explored the potential of locked nucleic acid (LNA)-modified AON gapmers in combination with a fibrin hydrogel bridging material to induce gene silencing *in situ* at a SCI lesion site. LNA gapmers were effectively developed against two promising gene targets aiming at enhancing axonal regeneration—RhoA and GSK3β. The fibrin-matrix-assisted AON delivery system mediated potent RNA knockdown *in vitro* in a dorsal root ganglion explant culture system and *in vivo* at a SCI lesion site, achieving around 75% downregulation 5 days after hydrogel injection. Our results show that local implantation of a AON-gapmer-loaded hydrogel matrix mediated efficient gene silencing in the lesioned spinal cord and is an innovative platform that can potentially combine gene regulation with regenerative permissive substrates aiming at SCI therapeutics and nerve regeneration.

INTRODUCTION

Spinal cord injury (SCI) is among the most daunting challenges for regenerative medicine. It can lead to considerable damage to the human motor and physiological functions, having a significant impact on the quality of life and life expectancy, with high costs associated with primary care and loss of income. To date, there are no effective treatments to reverse the damage to the spinal cord.

Several factors contribute to the non-permissive environment formed at the injury site that is responsible for the limited neuroregeneration and recovery observed after a SCI,[1] including the formation of a glial scar containing inhibitory extracellular matrix molecules released by reactive astrocytes.[2,3] Also, the presence of myelin debris, accumulated due to the damage to oligodendrocyte myelin structures and subsequent inefficient clearance by phagocytic inflammatory cells, contributes to the inhibitory environment responsible for impeding axonal regeneration.[4,5] As such, therapeutic strategies that can block the inhibitory signaling cascades promoted by the non-permissive environment formed after SCI could have a positive impact on regeneration. Some approaches are already being investigated, even in clinical trials, involving the use of blocking antibodies (e.g., anti-NogoA), peptides (e.g., NEP1-40), and enzymes (e.g., C3-transferase, chondroitinase ABC), among others.[6,7] Nonetheless, the inhibition of genetic targets through the use of antisense oligonucleotides (AONs) could offer a new or complementary approach to existing options.

Compared to conventional drugs, AONs have an increased degree of specificity since the interaction with their targets is based on the genetic code. Furthermore, their design obeys a more "rational" approach, as their RNA-binding activity is governed by Watson-Crick rules instead of computational approaches for studying protein-small molecule interactions.[8] This Watson-Crick "rationale" also makes any newly identified target gene virtually immediately addressable by an antisense agent. Moreover, inhibition of mRNA expression produces quicker and longer lasting clinical responses than protein inhibition by conventional drugs. This is explained by both the recycling nature of the mechanism of mRNA degradation elicited by RNase H-based AONs and the resistance to both extra- and intracellular degradation by newly developed AON chemistries, which most often surpass those afforded by recombinant proteins, peptides, and antibodies.[9,10] Of interest, when in the CNS, most AONs are readily taken up by neurons and glia,[11–13] although the exact mechanisms of uptake are still under investigation.[14–16] A

Received 9 June 2017; accepted 15 March 2018;
https://doi.org/10.1016/j.omtn.2018.03.009.

[9]These authors contributed equally to this work.

[10]Present address: Division of Cancer Research, University of Dundee, Dundee, DD1 9SY, UK.

Correspondence: Ana P. Pêgo, PhD, INEB - Instituto de Engenharia Biomédica, Universidade do Porto, 4200-135 Porto, Portugal.
E-mail: apego@ineb.up.pt

particular advantage of AONs targeted to the CNS has been their exceptionally long half-lives, which is of relevance for situations where prolonged effects are desirable, avoiding the need for repeated (invasive) administrations. This has been demonstrated in the case of downregulation of mutant huntingtin (m*HTT*), with suppression of mRNA lasting for up to 12 weeks in mice and in non-human primates.[17] Additionally, further support for the long AON half-lives in the CNS is given by clinical data from amyotrophic lateral sclerosis (ALS) patients in whom AONs, after intrathecal administration, could be detected for up to 3 months in the spinal cord and brain.[18]

In the context of a CNS lesion, such as a SCI, the functional delivery of modified AONs is still rather unexplored, as is its potential for combinatorial approaches using biomaterials capable of bridging the injured areas.[1] To this regard, fibrin materials have been explored in combination with nanoparticle systems for purposes of *in situ* gene therapy applications.[19–21] Importantly, fibrin hydrogels have been reported to improve functional recovery after SCI by acting as a permissive bridging material for axonal regeneration when applied to the lesion site.[22–25] However, the specific combination of fibrin hydrogels with AONs has never been reported. In fact, the possibility of exploring a local application of the AONs is highly beneficial in this context to confine its action to the site of interest (lesioned area).

Thus, in this work, we explored the combination of a fibrin hydrogel bridging material that not only will provide a scaffold for tissue regeneration but also will serve as a reservoir for locked-nucleic-acid (LNA)-modified AON *in situ* delivery and the downregulation of relevant gene targets in a SCI context. LNA AONs have been used in many different settings such as antisense gapmers, anti-microRNAs (antagomiRs), and anti-gene approaches.[26–28] LNA gapmers have also been shown to have a remarkable gymnotic uptake *in vitro* and *in vivo*[29] and, additionally, in the CNS; and particularly in the brain, LNA-modified AONs were shown to be well tolerated.[30] As proof of principle, we designed AONs against genes associated with neurite outgrowth inhibition or with the intrinsic capacity to modulate neuronal regenerative programs in the context of SCI. Namely, LNA gapmers were designed against the Ras homolog gene family member A (RhoA), recognized as a key player in the inhibitory signaling cascade activated by the extracellular environment at a spinal cord lesion site,[31–33] and glycogen synthase kinase 3 beta (GSK3β), the inactivation of which has been shown to positively contribute to enhance the intrinsic axon regenerative potential, including axonal outgrowth through the glial scar.[34–36] Although achieving nerve regeneration is considered a multifactorial process, the choice of these gene targets was based on previous therapeutic approaches, using modalities other than AONs, that either reached clinical trials or had their potential confirmed by pharmacological inhibition in *in vivo* settings[37,38]. Many other targets have been presented with the potential to increase the regenerative potential of neurons[39] and can thus be amenable to AON-based strategies.

Still, as these genes have broad physiological functions, it further strengthens the importance of developing an effective but controlled and localized delivery of the antisense drug. We further show that AONs remain within fibrin hydrogels, possibly by interacting with fibrin fibers, and that the hydrogel system mediates the successful delivery of functional LNA-based AON gapmers in a dorsal root ganglion (DRG) explant 3D culture system. Moreover, we provide evidence that the system can be used *in vivo* and applied to a SCI, thus promoting the local downregulation of relevant target therapeutic genes. By circumventing a systemic or intrathecal administration and directly targeting the site of interest, we hypothesize that the use of higher dosing regimens of therapeutic AONs can be avoided, thereby lowering the associated costs and mitigating possible safety issues. Our results suggest the viability of locally applying modified AONs as efficient therapeutic drugs mediated by materials providing structural support in a spinal cord lesion, as a novel SCI therapeutic approach.

RESULTS

Design and Evaluation of Antisense Oligonucleotide Gapmers (2′-*O*-Methyl and LNA Based) Targeting *RhoA* and *Gsk3β*

For the design of AONs against the two target genes of interest—*RhoA* and *Gsk3β*—an algorithm from Integrated DNA Technologies (IDT) was used, as well as IDT OligoAnalyzer tools (http://eu.idtdna.com/calc/analyzer), to check for self-annealing and discard AON sequences with low melting temperature (Tm; 55°C was chosen as the cutoff, using the default conditions against RNA target, from IDT OligoAnalyzer) and BLASTn[40] for specificity checks. An AON gapmer[41] design was chosen using 2′*O*-Me RNA bases at the 5′ and 3′ ends for the initial screening. A set of six different 22-nt ASOs, targeting rat *RhoA* and *Gsk3β* were chosen to be evaluated regarding their downregulation efficiency *in vitro*. After transfections into a rat Schwannoma cell line (RN22), several AONs against each target were identified as being able to promote a >70% downregulation level (Figure 1).

The AON showing the highest activity, in the initial screen, for each gene (*Gsk3β* and *RhoA*) was chosen to be modified to an LNA gapmer (AON 183 and AON 180, respectively). Additionally, for *Gsk3β*, one extra AON (AON 026) was chosen for LNA gapmer substitution, while for *RhoA*, three other AONs were chosen for LNA gapmer substitution (AON178, AON 180, and AON 024), as there was higher variance in knockdown potency in the RhoA AON groups in the preliminary *in vitro* 2′-*O*-methyl gapmer activity experiments. After *in vitro* screening, one LNA AON for each target was identified as having strong potential for gene downregulation (Figure 2), namely, LNA6624 against *Gsk3*β and LNA6621 against *RhoA*.

Characterization of the Microstructure of AON-Loaded Fibrin Hydrogels and AON Release Kinetics

For *in situ* delivery of AONs, a fibrin hydrogel vehicle was used. Two concentrations of fibrinogen were chosen to make the hydrogel—namely, 6 and 14 mg/mL. A fully thiolated 2′-*O*-methyl RNA single-stranded control oligonucleotide (Cy5-AON) was used as a model AON to study incorporation in the fibrin hydrogels and its possible derived effects to the fibrin meshwork. The fibrin gel structure, with

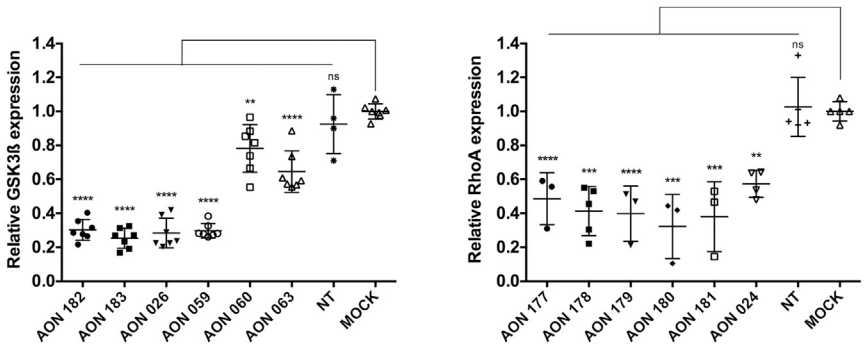

Figure 1. Screening of 2′-O-Methyl RNA/DNA Gapmer AON Sequences for Downregulation of GSK3β and RhoA

Relative expression levels were analyzed by qRT-PCR, after transfection of the different LNA gapmers (at a final concentration of 0.3 μM) into the RN22 cell line. Results indicate mean ± SD, with each data point representing one transfection. Statistical significance was determined using one-way ANOVA, followed by Tukey multiple-comparison test (**$p < 0.01$; ***$p < 0.001$; ****$p < 0.0001$; ns, not significant).

and without AONs, was evaluated using FITC (fluorescein isothiocyanate)-labeled fibrinogen and Cy5-AON (Figure 3). Interestingly, the fibrin network density decreased when the gel was formed in the presence of AONs, as shown by the ∼2-fold increase in the average pore area (Figure 3A). In addition, we observed that the AONs were distributed almost exclusively along the fibrin fibers, as revealed by the extensive fluorescence co-localization (Figure 3B). This could explain the decreased fibrin network density while suggesting a promising role for the fibrin gel as an AON vehicle for local sustained delivery. The incorporation of the control AON (Cy5-AON) in the fibrin gels impacted the fibrin network structure, resulting in enhanced neurite outgrowth from DRG explants when compared with gels without AONs (Figure S1). Such behavior is in line with the effect observed in gels with increased pore size that mediate enhanced neurite extension.[42]

Finally, AON release from fibrin gels was assessed *in vitro* in Tris-buffered saline (TBS) at 37°C (Figure 4). The cumulative release (Figure 4A) over 3 days of incubation, with total medium exchange at each time point (sink conditions), reached almost 90%, without attaining a plateau, showing that the AONs are still diffusing, despite the observed close interaction between AONs and fibrin fibers. When the gels were incubated in the presence of the release buffer without any buffer exchange, a high retention of AONs was obtained with around 65% AON being retained after 24 hr and 55% after 72 hr.

When using sink conditions, the successive exchange of buffer stimulates a fast release of the AONs by diffusion, as the gel maintains integrity throughout the incubation period. In the second condition, without buffer replacement, diffusion of the AONs occurs much more slowly. An initial release of 20% AON with 2 hr of incubation was observed, with a total of 40% AON being released when incubated for 72 hr. As the initial AON concentration in the gel was 6 μM, the initial 20% release into the buffer (with 10× the volume of gel) would correspond to a concentration of 0.12 μM in the buffer solution and 0.24 μM (corresponding to 40% release) after 72 hr. This indicates that an equilibrium of the AON between the gel-solution phases should not be the main cause of the high retention of the AON in the gel.

Fibrin Gels Support the Functional Delivery of Free LNA AONs in an *In Vitro* DRG Explant 3D Culture System

After establishing and characterizing our AON-loaded fibrin gel system, we next cultured DRG explants embedded in a gel loaded with Cy5-AON. This enabled the study of AON uptake in primary neuronal cells accounting for the influence of a 3D microenvironment. Forty-eight hours after the incubation start, a homogeneous distribution of the AONs was found throughout the explant (Figure 5A), with uptake of AONs by neuronal cells verified by the co-localization of the Cy5 fluorescence with β-III-tubulin (neuronal marker)-stained cells (Figures 5B–5E).

Next, LNA AONs against the targets of interest (*Gsk3β* and *RhoA*), and an unrelated sequence (GFP), were incorporated in the fibrin gel to assess functionality. DRG explants were embedded in the AON-containing gels, and after 7 days of culture, RNA and protein levels were determined. A significant and specific gene downregulation, both at the RNA (around 50%–60%) and protein levels (around 70%), was achieved, thus confirming the bioactivity of the AONs released from the fibrin gel (Figures 6 and S2).

Fibrin Gels Support the Delivery of Functional Free LNA AONs in a Rat Model of SCI

We utilized the hemisection model system to perform the *in vivo* studies, as transection models are particularly useful in regenerative medicine research.[43] The strategy (Figure 7A) consisted of the application of antisense LNA-loaded fibrin gel into the lesion site in two subsequent layers, which was then covered by a bilayer P(TMC-CL) patch. The bilayer patch comprised a solvent cast film onto which electrospun aligned fibers have been deposited. Its use aimed at containing and isolating the lesion area, with the additional benefits of P(TMC-CL) being a known modulator of inflammation and positively influencing nerve regeneration when neurons are in contact.[44,45]

We initially checked for the distribution of the AONs 5 days post-lesion, using Cy5-AONs, and observed that the AONs were distributed throughout the lesion site and to regions distal from the lesion epicenter (with a tendency for caudal distribution at this time point) (Figure 7B), being found in close association with different cell types

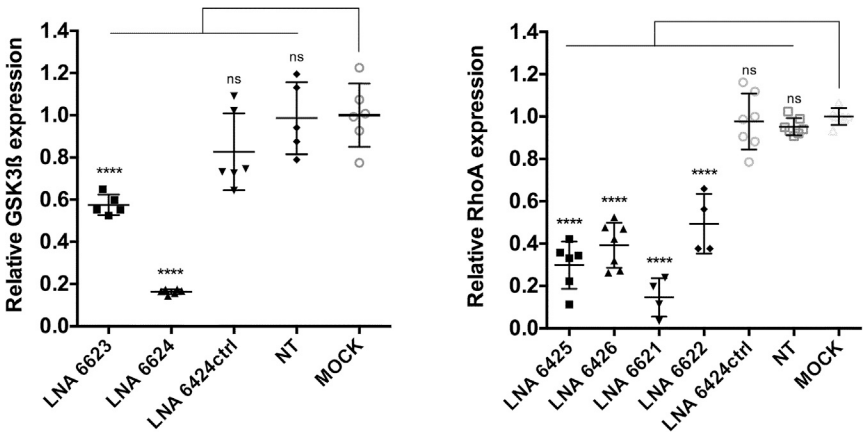

Figure 2. Screening of LNA Gapmer Sequences for Downregulation of GSK3β and RhoA

Relative expression levels (to mock-treated cells) were analyzed by qRT-PCR, after transfection of the different LNA gapmers (at a final concentration of 0.3 μM) into the RN22 cell line. Results indicate mean ± SD, with each data point representing one transfection. One-way ANOVA, followed by Tukey multiple-comparison test, was used for statistical analysis (****$p < 0.0001$; ns, not significant).

present (Figure S3). Next, at the same time point, a 1-cm length of spinal cord tissue (centered at the lesion site) was removed, and RNA was extracted for quantification of gene expression (Figure 7C). Here, antisense LNA-based oligonucleotides against *Gsk3β* were tested. Confirming the *in vitro* DRG experiments, a robust *Gsk3β* downregulation could be achieved (mean downregulation, 75%). Contrary to the *in vitro* experiments, a tendency for downregulation of *Gsk3β* was observed for the control LNA-GFP (around 47% knockdown), whereas using a second control AON (LNA-Luc) did not induce GSK3β downregulation. For this reason, we further inspected possible binding events of the LNA-GFP not only to the rat *Gsk3β* RNA transcript but now including all of its genomic sequence taken from the Ensembl database (ensembl genome browser release 91: https://www.ensembl.org/index.html). This takes into consideration recent reports stating the importance of the binding events of gapmer oligonucleotides to pre-mRNA and its influence in off-targeting.[46–48] One site in intron 1 of *Gsk3β* was found with only 2 mismatches to the LNA-GFP used. The found sequence (complementary to the LNA-GFP) was: GACGTAAA**tGa**CCA (mismatches in small letters), having two mismatches outside of the LNA wings. This points to a potential RNase H1 cleavage event at the pre-mRNA level that could lead to some level of downregulation of the final *Gsk3β* transcript.

We further observed the extent of the inflammation area to assess the initial implications of the system and possible negative effects of a localized bolus delivery of AONs into the spinal cord. Our observations revealed no increase of the inflammation area in animals receiving AON-loaded fibrin versus those treated with fibrin gel only, as checked by immunofluorescence staining of infiltrated microglia/macrophages ($IBA1^+$ cells) (Figure 8) and by H&E staining (Figure S4).

DISCUSSION

Single-stranded AONs currently offer several means of altering the expression of a target gene/RNA, such as through the direct blocking or degradation of a target transcript, redirection of pre-mRNA splicing patterns or blocking of microRNA function.[49] Through these mechanisms, AONs can ultimately regulate cell behavior, promote cell viability, and restore or alter cell function. The relative simplicity of their design, development, and use, allied with their multiple modes of action, confers a high therapeutic potential that is already being explored in a number of applications, including neurodegenerative disorders,[50] immunodeficiency,[51] cancer,[52] and cardiovascular and metabolic diseases,[53,54] with some at advanced clinical trial phases and even US Food and Drug Association (FDA) approved.[55,56] This therapeutic versatility prompted us to explore the application of AONs in the context of CNS nerve regeneration, specifically in a setting of SCI. In particular, with the understanding of the molecular pathways leading to inhibition of nerve regeneration, blocking of such inhibitory signaling by AONs could become a potent therapeutic strategy.[57] To this end, two molecular targets, *RhoA* and *Gsk3β*, were chosen as candidate genes for downregulation, as their inhibition has been shown to be relevant for promoting nerve regeneration.[36,37]

In general, application of AONs in the CNS normally involves bypassing the blood-brain-barrier (BBB) through intraventricular or intrathecal injections.[17,18] The intrathecal delivery through osmotic pump infusion[58] or intravenous injection[59] has also been reported in a few examples dealing with the application of AONs specifically in the context of SCI. Nevertheless, a more localized delivery system would be of benefit, especially when combined with a biomaterial-based scaffold that can serve as a mean to bypass the glial scar.[1] To this end, fibrin-based hydrogels have been shown to both provide a physical support and act as stimulant for axonal regeneration.[24,60] Moreover, fibrin gels can be loaded with drugs, protein growth factors, and gene-based nanocomplexes,[19,61,62] providing a delivery matrix for local application at a SCI lesion site. Nevertheless, gene-based or antisense approaches mediated by fibrin have not been widely investigated for application in SCI.[63] Such system can potentially allow a synergistic action between the pro-regenerative impact of the fibrin gel and the modulation of molecular mechanisms and cellular function mediated by the antisense gene therapeutics.

Here, we propose and characterize AON-loaded fibrin hydrogels and further investigate the efficiency of delivering potent LNA-modified AONs, unassisted by delivery vectors, mediated by the fibrin gel matrix at a SCI lesion site.

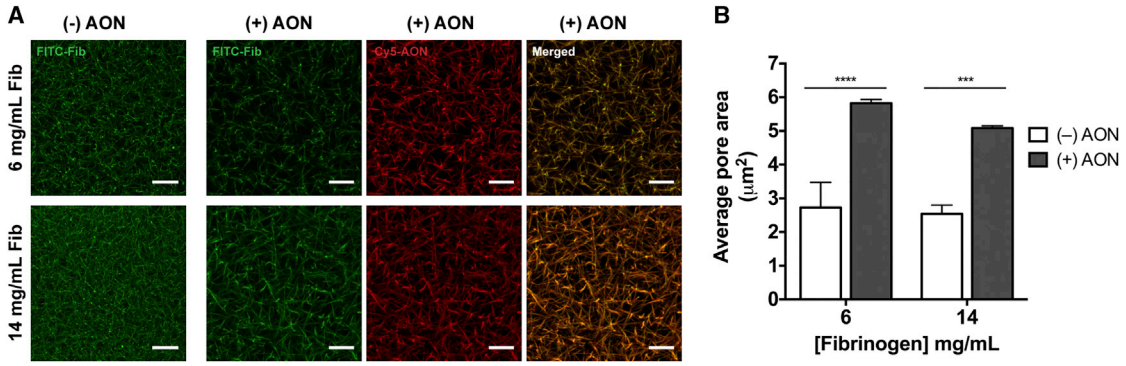

Figure 3. Characterization of the Fibrin Gel Network in the Absence or Presence of AONs

(A) Representative maximum Z-projections of confocal stack images of the corresponding fibrin gels (at fibrin concentrations of 6 and 14 mg/mL containing 1% (w/w) FITC-Fibrinogen). Complete association (co-localization) of Cy5-AONs with fibrin fibers (FITC-Fib) is observed. Scale bars, 10 μm. (B) Pore area was analyzed from confocal microscopy images taken from the fibrin gels. The maximum Z-projections were used to calculate the average pore area per image field using MATLAB. Two-way ANOVA, followed by Bonferroni post hoc test, was used for statistical analysis (mean ± SD; n = 3 image fields per gel; ****$p < 0.0001$; ***$p = 0.0001$).

The design of LNA-containing AON gapmers allowed the reduction of the size of the AONs, aiming at maintaining the same level of potency or even improving it.[29,41,64]

The embedment of the AONs on the fibrin gel matrix revealed that the gel network was influenced by the presence of the AONs, as the average pore area was significantly increased. This fact is already of importance to any studies that could use oligonucleotides loaded in fibrin gels for observation of neurite outgrowth lengths, as the sole physical impact of the AONs on the fibrin network density will influence neurite extension. One possible explanation could be the known tendency for oligonucleotides containing a phosphorothioated (PS) backbone to inhibit the thrombin clotting activity through a direct competition with fibrinogen for binding to exosite I of thrombin.[65] In addition, when using both fluorescently labeled AONs and labeled fibrinogen, we did not observe a diffuse fluorescence throughout the gel; instead, AONs were seen completely associated with the fibrin fibers. This could also be justified by the polyanionic nature of oligonucleotides, similar to the anticoagulant heparin, suggesting the potential of AONs to bind to the heparin-binding domain of fibrinogen (rich in positively charged amino acids) through weak electrostatic interactions.[66] While these features could mediate a potential negative effect if the PS AONs were to be delivered systemically in high doses, in the present context, these can be beneficial, as the fibrin fibers will act as natural local depots for the AONs, enabling an efficient loading of these relatively small oligonucleotide drugs (normally with an average molecular weight ranging from 4 to 8 kDa). Based on these observations, it could be expected that the electrostatic-force-mediated entrapment of the AONs within the fibrin network would impact the AON release kinetics from the fibrin hydrogels. Release tests have been conducted, both under non-sink and sink conditions. The observed kinetics further support the occurrence of a physical interaction between the AONs and the fibrin fibers (possibly of electrostatic nature), which enables some resistance to simple diffusion of the small AONs through the gel.

To confirm the bioactivity of the AONs after release, we incubated DRG explants embedded in AON-loaded gels. The use of DRG explants embedded in the fibrin gel allowed us to have a 3D *in vitro* system with primary neural cells in the presence of natural extracellular matrix components, thus mimicking free AON uptake in a microenvironment closer to the *in vivo* situation.[67–69] Under these conditions, we could confirm that the released AONs were bioactive, achieving a significant downregulation of the target genes of around 50%–60%.

The feasibility of using the AON-fibrin gel system was also evaluated in an animal model of SCI. For this, we used a hemisection of the rat spinal cord, which is commonly used to test hydrogel scaffolds and regenerative medicine therapies in general and is amenable to standardization aiming at reducing variability between lesions.[25,43] An initial amount of AON-loaded fibrin gel was allowed to polymerize *in situ* in order to better fill the lesion site, after which, a pre-polymerized AON-fibrin gel was placed directly atop the first gel to provide an extra reservoir of bioactive AONs. As pre-polymerized fibrin gels are more resistant to degradation,[24] this could provide an opportunity for the release of AONs over a longer period of time after the initially applied fibrin gel has been degraded. The diffusion of AONs in the lesion was assessed by visualization of Cy5-AONs 5 days following implantation. AONs were seen present at the lesion site at high levels (seen by the strong fluorescence), but also, an effective distribution throughout the lesion site and to regions distal from the lesion epicenter (with a strong tendency for caudal distribution at this time point) was detected. Important was the observation that the AONs were not confined to the lesion epicenter, where the gel is initially applied, but were able to diffuse some distance into the intact spinal cord, an observation that, to the best of our knowledge, has not been reported yet. It is expected that several cell types can uptake the AONs in the CNS, as previously reported;[11–13] this can, in fact, be advantageous as some gene targets have been shown to have an widespread upregulation at a CNS lesion site.[39] For example, Rho A has been shown to be rapidly activated after trauma in the CNS, a cellular

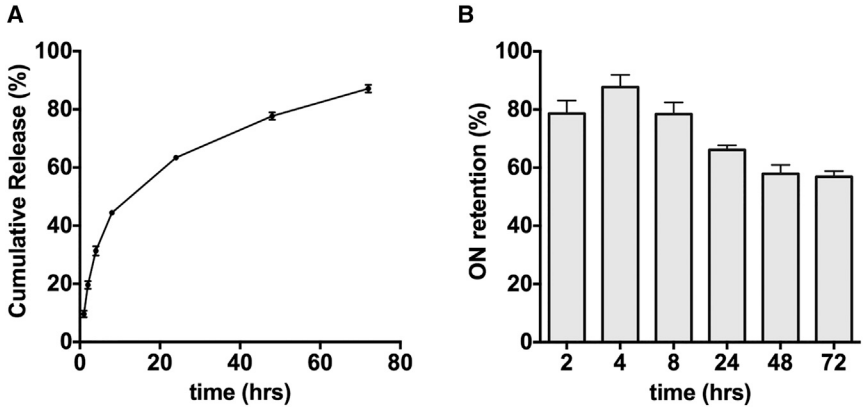

Figure 4. AON Release Behavior

(A) Cumulative release profile of AONs from fibrin hydrogels, *in vitro*. Cy5-AON loaded fibrin hydrogels (20 μL; 14 mg/mL fibrinogen) were incubated at 37°C in 200 μL TBS (pH 7.3) for 1, 2, 4, 8, 24, 48, and 72 hr. At each time point, the buffer was completely exchanged (sink conditions). (B) AON retention as a function of time was defined as the percentage of AON present in the gel in relation to the loaded mass. Cy5-AON loaded fibrin hydrogels (20 μL; 14 mg/mL fibrinogen) were incubated at 37°C in 200 μL TBS (pH 7.3). For each time point, one independent gel drop was used. Error bars indicate mean ± SD (n = 3 gel drops).

response conserved in various cells and regions of the CNS.[70] Thereby, affecting different nervous system cell types such as neurons or glia can have beneficial effects.[33,71]

Accordingly, the LNA AONs locally applied through the fibrin gel matrix were able to potently downregulate (around 75% inhibition) the expression of the target gene, *Gsk3β*, 5 days post-implantation of the gel at the spinal cord lesion site. We observed that, *in vivo*, the control LNA-GFP showed an unexpected effect leading to a decrease of the GSK3β levels, albeit at a lower level than the specific LNA-GSK3β. One site in intron 1 of *Gsk3β* pre-mRNA was found with only two mismatches against the corresponding LNA-GFP. This sequence contained two mismatches outside of the LNA wings, meaning that it could, indeed, act as antisense to the *Gsk3β* pre-mRNA. A study by Kamola et al.[72] using 16-mer LNA-modified AONs has shown active intron off-targets to be, in many cases, highly potent and that around 50% of putative intronic off-targets with 2 mismatches showed very significant knockdown, with some sequences even displaying knockdown activities equivalent to those of the on-target AONs. Even for 14-mer LNA-modified AONs with 2 mismatches, a significant number of interactions were reported as still occurring.[72] The question of how accessible this site is—and, thus, the strength of knockdown—is hard to predict *in silico* with current available tools, but this information provides a strong basis to explain the downregulation observed *in vivo*. The mismatches in this case are located in the DNA region of the gapmer and not in the LNA wings. Although this could suggest that the penalty in Tm could be lower than if mismatches were located in the LNA region, such inference is, in reality, difficult to foresee, further complicating the analysis of the off-targeting potential of AONs.[73]

It is worth noting, however, that *in vivo*, we are using a much higher concentration of oligos than in the *in vitro* screens.

Also, by using a second control LNA-AON sequence (LNA-Luc, found to have at least ≥ 3 mismatches against the *Gsk3β* pre-mRNA), such downregulation effect was not present, corroborating the initially unforeseen specific effects of the LNA-GFP sequence. The effect observed with the control oligo LNA-GFP attests to the importance of a careful investigation of possible off-target binding events leading to RNase-H-mediated antisense effects at the pre-mRNA level by modified gapmer AONs, as recently reported.[47,48,72]

Also importantly, in the lesioned spinal cord, acute tissue toxicity differences between animals treated with fibrin only or fibrin with *Gsk3β* or GFP LNA gapmers were not observed. In fact, the inflammation status of the injury area 5 days post-implantation of the AON-fibrin gel system was qualitatively evaluated by looking at the presence of microglia/macrophages in the different experimental conditions, as well as by H&E staining. The presence of microglia/macrophages was observed in all the conditions (fibrin only, fibrin/LNA-GSK3β, and fibrin/LNA-GFP), which is in agreement with previous reports where fibrin was shown to be permissive to cell migration and infiltration.[24] Furthermore, no notable alterations in terms of inflammation response could be observed in the LNA-GSK3β-treated animals when compared to both the fibrin-only and control fibrin/LNA-GFP AONs, indicating that the presence of AONs did not exacerbate this response.

We thus propose that the delivery of free AONs from a fibrin gel matrix is a viable option for SCI application, potentially providing a combinatorial effect where the AONs are able to locally modulate cellular gene expression, while fibrin hydrogel offers a permissive support matrix for cell infiltration and neuronal regeneration.

MATERIALS AND METHODS

Synthesis of Oligonucleotides

2′O-Methyl RNA-DNA AON Gapmers

All 2′*O*-methyl RNA-DNA AON gapmers were synthesized on an ÄKTA Oligopilot Plus 10 system at GE Healthcare Bio-Sciences (Uppsala, Sweden) using Primer Support 5G UnyLinker (353 μmol/g) as solid support. Standard template 2′-*O*Me RNA synthesis methods were used except thiolation, which was carried out with a 1:1 mixture of acetonitrile (ACN) and 0.2 M PADS ((bis(diphenylacetyl)disulfide) (Ionis Pharmaceuticals, Carlsbad, CA, USA) in ACN/3-Picoline 1:1 [v/v]). Other ancillary reagents (EMD Chemicals, Gibbstown, NJ,

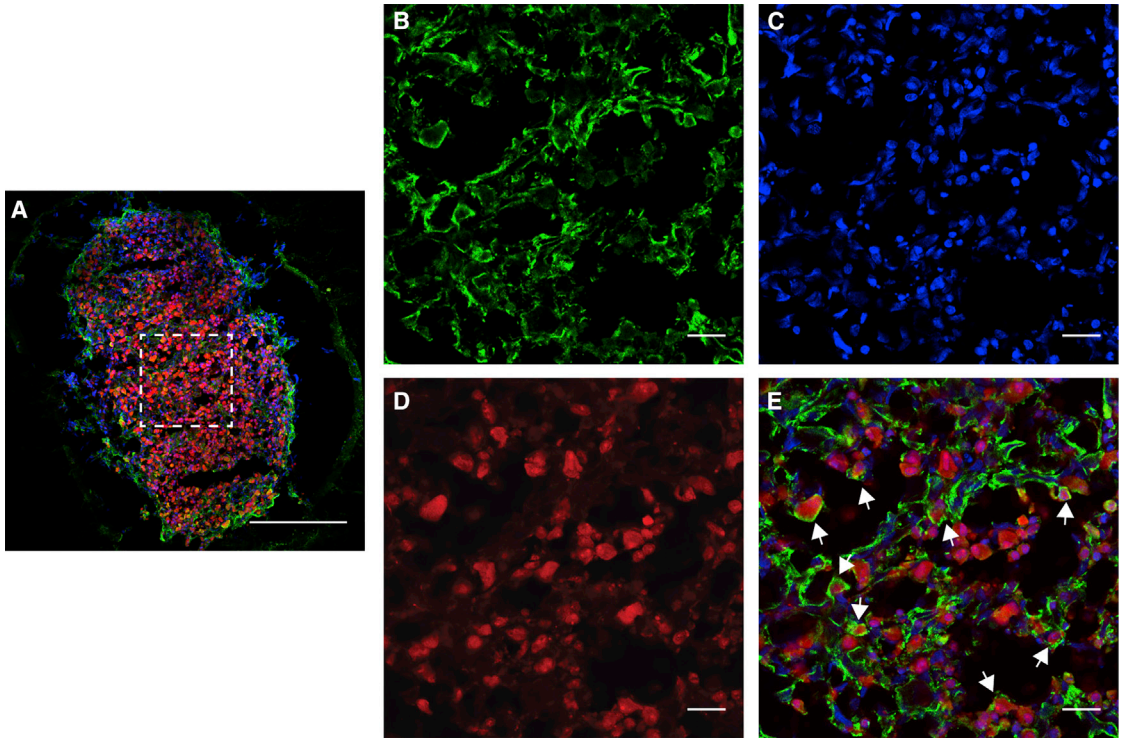

Figure 5. Distribution of Naked AONs in a DRG Explant

DRG were cultured in a fibrin gel (14 mg/mL Fibrinogen) containing 6 μM of AONs and cultured for 48 h. DRG were processed by cryosectioning and images represent the middle section (in Z axis) imaged by confocal laser scanning microscopy (CLSM). (A) A MAX intensity Z-projection of the whole DRG middle section (16 μm thick) with the following staining: β-III tubulin (green); Cy5-ON (red); and nucleus (blue). The white square delimits the area observed in (B)–(E) (β-III tubulin, green, B; nucleus, blue, C; Cy5-AONs, red, D; merged picture, E). (B–E) The cellular distribution of the AONs in neuronal (β-III tubulin stained) and non-neuronal cells (representative examples of β-III-tubulin-stained neuronal cells with intracellular ONs are indicated with arrowheads). Scale bars, 200 μm in (A) and 20 μm in (B)–(E).

USA) were used as recommended by GE Healthcare Bio-Sciences. Cy5 amidite (GE Healthcare, #28904249) was used as recommended by the supplier. Final detritylation and dietylamine treatment were carried out (to remove beta-cyanoethyl groups) prior to cleavage and deprotection overnight in 25% aqueous ammonium hydroxide (Merck, Darmstadt, Germany) at 55°C, releasing the crude oligonucleotide derivative into solution ready for purification.

All purifications were carried out using an ÄKTAexplorer 100 system equipped with Capto Q ImPres columns for anion-exchange chromatography (AEC) (buffer A: 10% ACN, 10 mM $NaClO_4$, 50 mM Tris [pH 7.5]; 1 mM EDTA; buffer B: 10% ACN, 500 mM $NaClO_4$, 50 mM Tris [pH 7.5]; 1 mM EDTA).

After AEC purification, the AONs were in a solution containing sodium perchlorate. The salt was removed from the samples by gel filtration with an isocratic flow (3 mL/min) of Milli-Q water. Five HiTrap desalting columns were mounted in serial on the ÄKTAexplorer system and enabled desalting of one complete 12-mL fraction in about 15 min.

For purity analysis and characterization of the oligonucleotide derivatives, a Xevo G2 QTof, together with an AQUITY UPLC H-Class system (both from Waters Sweden, Sollentuna, Sweden) equipped with an ACQUITY UPLC OST C_{18}, 1.7 μm, 2.1-mm × 50-mm column (buffer A: 15 mM triethylamine [TEA]/400 mM hexafluoroisopropanol [HFIP] in water; buffer B: methanol [MeOH]), controlled by MassLynx was used, together with Maxent1 (Waters Sverige AB) software for molecular weight calculation.

LNA AON Gapmers

LNA AON gapmers were synthesized at the University of Southern Denmark on an ÄKTA Oligopilot Plus 10 system under anhydrous conditions using a polystyrene-based support in 1.0-μmol scale. LNA monomers were obtained from Exiqon A/S. The synthesis conditions used for the incorporation of LNA monomers were as follows: trichloroacetic acid in CH_2Cl_2 (3:97) as detritylation reagent; 0.25 M 4,5-dicyanoimidazole (DCI) in CH_3CN as activator; acetic anhydride in tetrahydrofuran (THF) (9:91, v/v) as cap A solution; *N*-methylimidazole in THF (1:9, v/v) as cap B solution; as a thiolation solution, 0.0225 M xanthan hydrate in pyridine/CH_3CN (20:90, v/v); coupling time was 6 min. Determination of the stepwise coupling yields (95%–99% per step) was based on the absorbance of dimethoxytrityl cations (DMT^+) released after each coupling step. The cleavage from the support was carried out by using a 32% (w/v) aqueous solution of

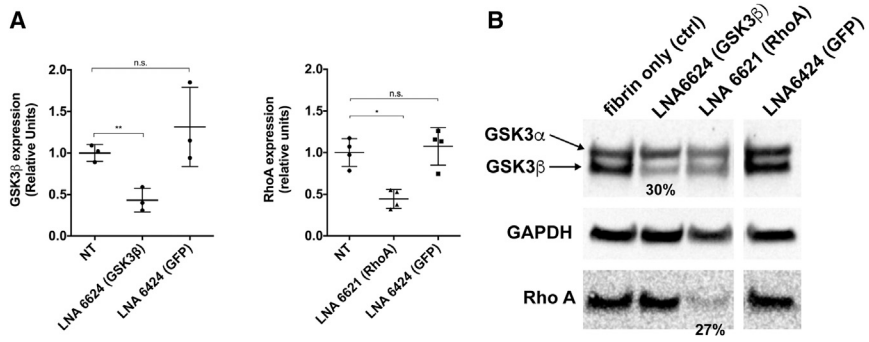

Figure 6. Downregulation of GSK3B and RhoA in DRG Explants

DRG explants were cultured within a 3D fibrin hydrogel loaded with LNA-AONs (6 μM inside the gel or 2 μM if related to final culture volume: gel/20 μL + culture medium/40 μL). 6 μM inside the gel or 2 μM if related to final culture volume: gel/20 μL + culture medium/40 μL. (A) Relative RNA quantification by qRT-PCR after a 7-day exposure to LNA AONs. LNA AONs against an irrelevant sequence (LNA6424-GFP) were used as controls. Each point represents an independent experiment where RNA from a pool of 10–15 independently treated DRG explants was used per condition and per independent experiment for qPCR quantification. Results indicate mean ± SD. One way-ANOVA with Dunnett's multiple comparison test (versus non-treated [NT]) was used where indicated (*$p < 0.05$; **$p < 0.01$; n.s., not significant). (B) Western blot analysis of GSK3β and RhoA protein expression levels after AON treatments. Protein was extracted from a pool of 10–15 DRG explants, each treated independently with LNA gapmers. Percentages shown indicate the relative amount of protein remaining in comparison to control and normalized to the GAPDH band, as calculated by semi-quantitative analysis (band densitometry). For the original western blot membranes, see also Figure S2.

ammonia for 12 hr at 55°C. All oligonucleotide products were purified by reversed-phase high-pressure liquid chromatography (RP-HPLC) using a Waters 600 system equipped with an XBridge OST C18 (2.5 μm, 19 × 100 mm) column and an XBridge Prep C18 (5 μm, 10 × 10 mm) pre-column. After DMT-group removal, the oligonucleotide products were further characterized by ion-exchange HPLC (IE-HPLC) on a Dionex HPLC system (VWR) and by MALDI-TOF on a microflex MALDI system (Bruker Instruments, Leipzig, Germany). The purified oligonucleotides were precipitated from acetone, and their purity (>90%) and composition were verified by IE-HPLC and MALDI-TOF analysis, respectively.

Oligonucleotide sequences and modifications are shown in Table 1.

Cell Culture and Transfections

The RN22 cell line (ECACC 93011414), a rat Schwannoma cell line, was cultured at 37°C, 5% CO_2, in DMEM with GlutaMAX (GIBCO), supplemented with 10% (v/v) heat-inactivated (30 min, 57°C) fetal bovine serum (FBS; GIBCO) and 30 μg/mL gentamycin (Sigma-Aldrich). All cell lines were routinely checked for Mycoplasma contamination.

Cells were seeded (75,000 viable cells per well; viable cells determined by the trypan blue exclusion assay) in 24-well plates 24 hr prior to transfections. At the day of transfection (with cells at around 75% confluency), culture medium was exchanged for medium without antibiotics. Transfections were conducted using the TransIT-Oligo Transfection Reagent (MirusBio). Briefly, 4 μL TransIT reagent was mixed with 50 μL serum-free Opti-MEM (GIBCO), after which 4.5 μL AON (20 μM) was added. The transfection mixture was incubated for 15–20 min before adding to the cells, in a final volume of 300 μL. An equal volume of complete medium (no antibiotics) was then added after 6 hr, and incubation proceeded for a total of 24 hr.

Preparation and Characterization of AON-Loaded Fibrin Gels

Fibrin hydrogels were prepared with human fibrinogen containing factor XIII (Sigma-Aldrich). Fibrinogen solution was prepared dissolving fibrinogen in ultrapure water, followed by dialysis against TBS (137 mM NaCl, 2.7 mM KCl, 33 mM Trizma base [pH 7.4]) for 24 hr. The resulting fibrinogen solution was then sterile-filtered, and its concentration was determined spectrophotometrically at 280 nm.[74] Fibrin gels were obtained by mixing equal volumes of the fibrinogen solution and a thrombin solution in TBS containing $CaCl_2$ and aprotinin (Sigma-Aldrich) (final concentration of fibrin components: 6 or 14 mg/mL human fibrinogen, 2 NIH U/mL [for *in vitro* experiments] or 25 NIH U/mL [for *in vivo* experiments] human thrombin, 2.5 mM $CaCl_2$, and 10 μg/mL [*in vitro*] or 25 μg/mL [*in vivo*] aprotinin in TBS). AONs were incorporated into the fibrinogen solution before mixing with the thrombin working solution. Fibrin gels were allowed to polymerize for at least 30 min at 37°C in a 5% CO_2 humidified incubator.

Fibrin hydrogel microstructure was analyzed by confocal laser scanning microscopy.[74] Fibrin gels (20 μL) were prepared as described earlier in a 15-well μ-Slide Angiogenesis (IBIDI) and hydrated with 40 μL PBS before image acquisition. To visualize the fibrin network, Alexa-Fluor-488-labeled human fibrinogen (Thermo Fisher Scientific) was mixed with non-labeled human fibrinogen at a 1:100 ratio (final concentration, 0.14 mg/mL). Cy5-labeled AONs (Cy5-AON705) were used to track AON distribution within the fibrin gel network. Images were acquired with a Leica TCS SP2 confocal microscope (Leica Microsystems, Wetzlar, Germany) with a 63×/1.4 oil-immersion objective lens and a zoom factor of 4. Three randomly chosen fibrin fields were analyzed at 0.5-μm step size to obtain 10-μm z stack images (1,024 × 1,024 × 172 pixels). Maximum Z-projections were then used to calculate the average fibrin pore areas per image field using MATLAB 8.6 (v.R2015b).

To assess the AON release from the fibrin hydrogel, Cy5-labeled AONs (Cy5-AON705) containing hydrogels (120 pmol AON in 20 μL) were incubated with 200 μL TBS at 37°C. Quantification of AON release was evaluated in two different ways: (1) at every time point, the buffer was completely removed and stored at −20°C, new buffer was added to the gel drops (n = 3 independent gel drops),

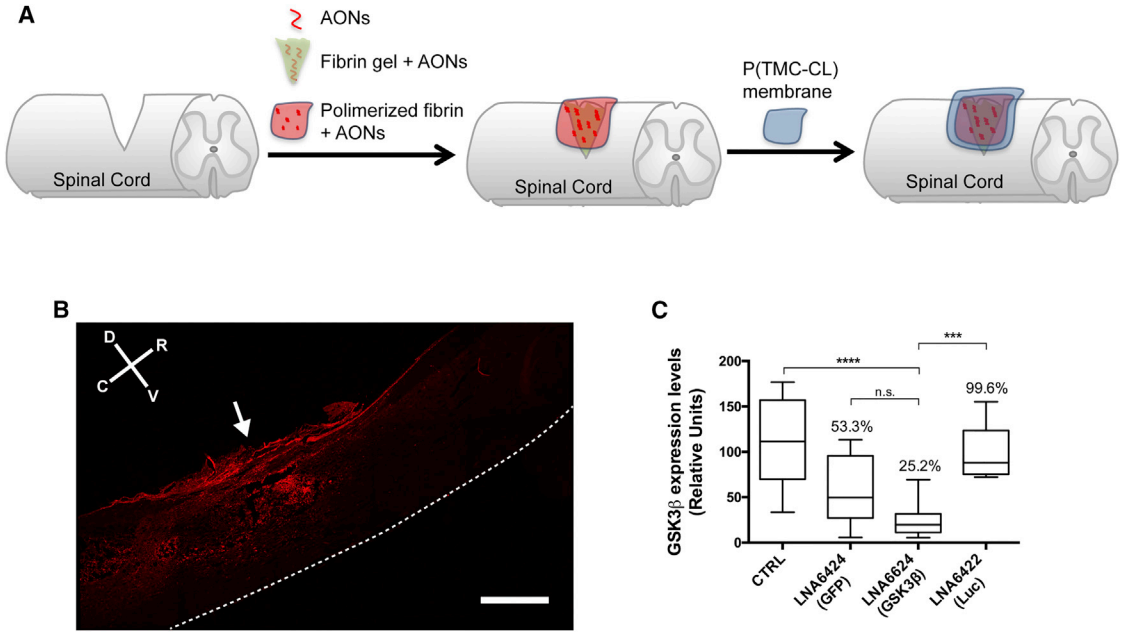

Figure 7. Downregulation of the GSK3β Target *In Vivo* after Delivery of Naked LNA AONs in a Fibrin Hydrogel System

(A) Schematic drawing of spinal cord injury hemisection model system and strategy for local release of antisense LNA-based antisense oligonucleotides (LNA AONs) from fibrin hydrogels. The hemisection lesion site is quickly filled with an AON-loaded fibrin gel (5 nmol) prior to polymerization, after which a pre-polymerized AON (5 nmol)-containing gel patch is placed covering the lesion. Finally, the AON-loaded fibrin gels were covered with a polymeric bilayer P(TMC-CL) patch to better hold the system in place and to retain AONs at the lesion site. (B) Distribution of Cy5-AON (red) along a spinal cord section 5 days post-application of the AON-loaded fibrin gels (white arrow points to location of the initial hemisection; dotted white line delimits the ventral side of the spinal cord). (C) Functional activity of LNA AONs after local application of the AON-loaded fibrin gel delivery system, evaluated 5 days post-lesion. Fibrin gel with no AONs was applied in the lesion of control group rats (CTRL). LNA AONs against GFP or Luciferase (LNA6424-GFP and LNA6422-Luc) were also used as additional controls. Relative quantification of GSK3β RNA levels by qRT-PCR is indicated. Values above box plots refer to GSK3β expression levels as relative mean percentages. Error bars represent minimum-maximum (min-max), with line at median (control, n = 9; LNA6624, n = 11; LNA6424, n = 11; LNA6422, n = 7). One-way ANOVA, with Tukey multiple comparison, was used for statistical analysis (***$p < 0.001$, ****$p < 0.0001$; n.s., not significant).

and at the end of the experiment, the AON present in all the samples was quantified by fluorescence reading in a multimode microplate reader (SynergiMX, Bioteck); (2) an independent gel drop per time point (n = 3 gel drops per time point) was used, with the buffer being removed and stored at −20°C (no buffer was added again). The gel drops were stored at −20°C and, at the end of the experiment, incubated with 0.25% Trypsin/0.05% EDTA for 30 min at 37°C to solubilize the hydrogel and release remaining AONs. AON release/retention was quantified by fluorescence readings as described earlier and expressed as a function of the fluorescence of AON-containing gel drops produced and immediately stored at −20°C (no buffer incubation step).

Animals

All animal experiments were carried out with the permission of the local animal ethical committee in accordance with the European Union (EU) Directive (2010/63/EU) and Portuguese law (DL 113/2013). The experimental protocol (421/000/000/2014) was approved by the ethics committee of the Portuguese official authority on animal welfare and experimentation (Direção-Geral de Alimentação e Veterinária; DGAV). DRG (*in vitro* studies) were obtained from rat embryos from pregnant 3-month-old female Wistar rats. Female Wistar rats (130–200 g) were used for the SCI surgeries. All animals were maintained under a 12-hr/12-hr light/dark cycle and fed with regular rodent's chow and tap water *ad libitum*.

DRG Explant Cultures

DRG explants were dissected from embryonic day (E)18 rat embryos and were temporarily maintained in ice-cooled DMEM/F12 with GlutaMAX (GIBCO) and 1% (v/v) P/S (Biowest). Fibrin gels (with or without 6 μM of AONs in the gel) were prepared as described earlier in 15-well μ-Slide Angiogenesis plates (IBIDI) and DRG explants embedded in the fibrin polymerizing solution (1 DRG /well), under a stereoscope. Fibrin was allowed to polymerize for at least 30 min at 37°C in a 5% CO_2 humidified incubator before the addition of 40 μL medium: (DMEM/F12 with GlutaMAX, supplemented with 2% [v/v] B-27 [Thermo Fisher Scientific), 1% (v/v) P/S, 1.25 μg/mL amphotericin B (Capricorn Scientific), 30 ng/mL NGF (Millipore), and 10 μg/mL aprotinin (Sigma-Aldrich). DRG explants were cultured for up to 7 days. Half volume of the medium was changed every 3 days. NGF was withdrawn at day 6 of culture. The distribution of AONs within the DRG was assessed at day 2 of culture by immunofluorescence, while mRNA and protein levels were determined at day 7 of culture.

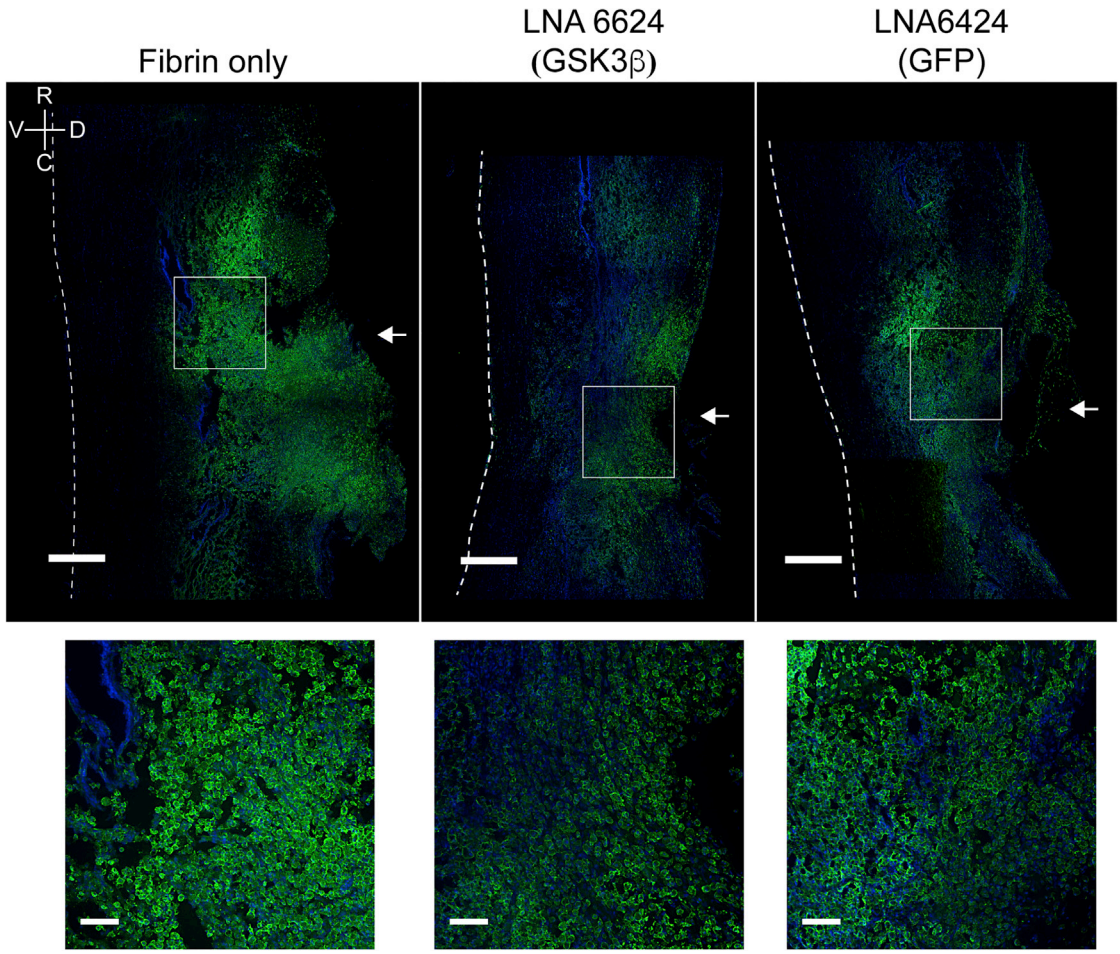

Figure 8. Inflammation Status of the Injury Area after Implantation of AON-Fibrin Gel

Inflammatory response as determined by IBA1 staining (monocyte/macrophage marker) of middle sections of the spinal cord 5 days post-implantation of the AON-loaded fibrin gel delivery system. White arrows point to the location of the hemisection; dotted line delimits the spinal cord at the ventral side. White squares represent the corresponding magnified areas shown on the lower picture panels. IBA1 staining (green), nucleus (blue). Scale bars, 500 μm (upper panels) and 100 μm (lower panels).

SCI Model: Surgeries

Female Wistar rats were anesthetized with a peritoneal injection of ketamine (75 mg/kg; Prodivet ZN) and medetomidine (0.5 mg/kg; Vétoquinol) or isofluorane (at 5% for induction and 1.5%–3% during surgery). Before surgery, animals received two separate subcutaneous injections of the analgesic buprenorphine (0.04 mg/kg; Richter Pharma Ag) and 3 mL saline solution with 5% (w/v) glucose or Ringer's lactate solution. The spinal cord was exposed by laminectomy at the T7/T8 level. The dura mater was then opened longitudinally, and a dorsal hemisection was performed at a depth of approximately 2 mm using a microscissor (reference no. 15025-10; Fine Science Tools). A solution of 5 μL fibrin gel with or without AONs (5 nmol) was then applied to the lesion and allowed to polymerize *in situ* (with gelification occurring in around 5 s) with a further pre-polymerized fibrin gel patch applied to the top of the lesion. Finally, a bilayer poly(trimethylene carbonate-co-ε-caprolactone) (P(TMC-CL)) patch, prepared as previously described,[44,75] was used to cover the lesion containing the fibrin gels. After this, the muscle and the skin layers were sutured. At the end of the surgery, only the animals anesthetized with ketamine/medetomidine were injected with atipamezole (1 mg/kg; Virbac). During all surgery procedures, the animal was kept on a heating pad to maintain the body temperature, and the eyes were constantly wet with a saline solution. In the following days, the animals were kept on a heating pad (2–3 days post-injury) and injected with buprenorphine (0.04 mg/kg). The bladder was manually emptied twice a day.

After 5 days, the animals were perfused through the left heart ventricle with 150 mL of 0.1 M PBS, followed by 4% (w/v) paraformaldehyde (PFA) in 0.1 M PBS, or they were sacrificed in a CO_2 chamber, and the spinal cord was removed and (1) processed for immunohistochemistry or (2) stored in RNAlater solution (Thermo Fisher Scientific), respectively.

Table 1. Oligonucleotides Used in the Study

Code	Target	Sequence
AON 177	*Rho A*	mU*mA*mC*mC*mU*mG*c*t*t*c*c*c*g*t*c*c*mA*mC*mU*mU*mC*mA
AON 178	*Rho A*	mA*mU*mC*mU*mU*mC*c*t*g*t*c*c*a*g*c*t*mG*mU*mG*mU*mC*mC
AON 179	*Rho A*	mC*mU*mC*mC*mC*mG*c*c*t*t*g*t*g*t*g*c*mU*mC*mA*mU*mC*mA
AON 180	*Rho A*	mA*mC*mC*mU*mC*mU*c*t*c*a*c*t*c*c*g*t*mC*mU*mU*mU*mG*mG
AON 181	*Rho A*	mC*mC*mG*mA*mC*mU*t*t*t*t*c*t*t*c*c*c*mG*mC*mG*mU*mC*mU
AON 024	*Rho A*	mA*mU*mC*mU*mC*mU*g*c*c*t*t*c*t*t*c*a*mG*mG*mU*mU*mU*mU
AON 182	*Gsk3β*	mA*mA*mA*mG*mG*mA*g*g*t*g*g*t*t*c*t*c*mG*mG*mU*mC*mG*mC
AON 183	*Gsk3β*	mC*mC*mU*mC*mA*mU*c*t*t*t*c*t*t*c*t*c*mG*mC*mC*mA*mC*mU
AON 059	*Gsk3β*	mG*mG*mU*mU*mC*mU*g*t*g*g*t*t*t*a*a*t*mG*mU*mC*mU*mC*mG
AON 063	*Gsk3β*	mC*mA*mG*mU*mU*mC*t*t*g*a*g*t*g*g*t*a*mA*mA*mG*mU*mU*mG
AON 060	*Gsk3β*	mG*mA*mG*mG*mA*mG*g*g*a*t*a*a*g*g*a*t*t*mG*mG*mU*mG*mG*mC
AON 026	*Gsk3β*	mU*mU*mC*mU*mC*mA*t*g*a*t*c*t*g*g*a*g*mC*mU*mC*mU*mC*mG
LNA 6425	*Rho A*	+T*+C*+C*t*g*t*c*c*a*g*c*+T*+G*+T
LNA 6426	*Rho A*	+T*+G*+C*c*t*t*c*t*t*c*a*+G*+G*+T
LNA 6621	*Rho A*	+C*+T*+C*t*c*a*c*t*c*c*g*+T*+C*+T
LNA 6622	*Rho A*	+C*+T*+T*t*t*t*c*t*t*c*c*+C*+G*+C
LNA 6623	*Gsk3β*	+A*+T*+C*t*t*t*c*t*t*t*c*t*+C*+G*+C
LNA 6624	*Gsk3β*	+C*+A*+T*g*a*t*c*t*g*g*a*+G*+C*+T
LNA 6424	GFP	+T*+G*+G*c*c*g*t*t*t*a*c*+G*+T*+C
LNA 6422	luciferase	+T*+T*+C*c*g*t*c*a*t*c*g*+T*+C*+T
Cy5-AON	β-globin (IVIS2-705)[a]	Cy5-*mC*mC*mU*mC*mC*mU*mU*mA*mC*mC*mU*mC*mA*mG*mU*mU*mU*mA*mC*mA

DNA bases are written in small letters; 2′-*O*-methyl RNA bases are written as mN (N, nucleotide); LNA bases are written as +N; phosphorothioate linkages are indicated by an asterisk.
[a]This oligonucleotide sequence was originally used for splice correction activity,[76] being targeted to the mutant form of β-globin (IVIS2-705). It was thus used as a control sequence having no relevant biological activity for this work.

RNA Extraction and qRT-PCR

RNA from cultured cells was extracted using Direct-zol RNA MiniPrep (Zymo Research). An amount of 200 ng RNA was used for the synthesis of cDNA using the NZY First-Strand cDNA Synthesis Kit (NZYTech). A final volume of 20 µL was used. qPCR was manually set up using the SYBR Green Supermix (Bio-Rad). The final reaction volume was 20 µL, using 2 µL cDNA from the RT step. Primers were used at a final concentration of 0.25 µM. Cycling conditions were as follows: hot start, 95°C, 3 min; PCR amplification (40 cycles), 95°C, 30 s (denaturation), 56°C for *Gsk3β*/*Ywhaz* or 55°C for *RhoA*/*Ywhaz* pairs, 30 s (annealing), and 72°C, 30 s (extension).

RNA from DRG explant cultures (pools of 10–15 DRGs) was extracted with the mirVana miRNA Isolation Kit (Ambion). Ten nanograms of RNA were used to manually set up the qPCR reaction using the SYBR Green One Step qPCR Kit (Biotools). The final reaction volume was 20 µL. Cycling conditions were as follows: reverse transcription, 50°C, 3 min; hot start, 95°C, 5 min; PCR amplification (40 cycles), 95°C, 10 s (denaturation), 56°C for *Gsk3β*/*Ywhaz* or 55°C for *RhoA*/*Ywhaz* pairs, 30 s (annealing) and 72°C, 20 s (extension).

For isolation of RNA from the spinal cord, 1 cm tissue (with the lesion as the center point) was homogenized in lysis buffer (mirVana miRNA Isolation Kit, Ambion), with the help of a tissue homogenizer (VDI 12, VWR) and/or a tissue grinder (1 mL; Wheaton). Samples were then processed afterward following the RNA isolation procedures as indicated (mirVana miRNA Isolation Kit, Ambion). An amount of 200 ng RNA was used for the synthesis of cDNA using the NZY First-Strand cDNA Synthesis Kit (NZYTech). A final volume of 20 µL was used. qPCR was manually set up using the SYBR Green Supermix (Bio-Rad) in conditions as described earlier.

Primers used were as follows: *Gsk3β* forward (Fwd) 5′-TCGAGTG GCGAGAAGAAAGAT, reverse (Rev) 5′- GTCTCGATGGCAGAT CCCAA; *RhoA* Fwd 5′-AATGAAGCAGGAGCCGGTAAA, Rev 5′-GATGAGGCACCCCGACTTTT; *Ywhaz* Fwd 5′-ACGACGTACT GTCTCTTTTGG, Rev 5′-GTATGCTTGCTGTGACTGGT. *Gsk3β* and *RhoA* mRNA expressions were normalized against the internal standard *Ywhaz*. All qPCRs were run on an iQ5 or CFX Real-Time PCR system (Bio-Rad), and data were calculated by the relative quantification method using the exponential transformation of delta Ct values ($2^{-\Delta\Delta Ct}$).

Primer efficiency was determined to be close to 100% based on standard curves using a known amount of RNA, which was serially diluted. Melt curves were always performed for checking primer

specificity. All samples were run in the qPCR plates as triplicates for each gene.

Western Blot

Protein was extracted from a pool of 10–15 DRG explants by lysis at 4°C in RIPA buffer (150 mM NaCl, 1% NP-40, 50 mM Tris [pH 8], 0.5% sodium deoxycholate, 0.1% SDS) supplemented with protease inhibitor cocktail (ref. P8340, Sigma-Aldrich). Total protein was quantified using the DC Protein Assay (Bio-Rad). Protein was loaded on a Bolt 4%–12% Bis-Tris Plus gel (Thermo Fisher Scientific) and run using MOPS buffer (Thermo Fisher Scientific) at 150 V for 50 min. Protein was transferred using an iBlot system (Thermo Fisher Scientific) equipped with a nitrocellulose transfer stack (Thermo Fisher Scientific) (P0 program used). Membrane was blocked in TBS-Tween 0.1% (v/v) with 5% (w/v) dry milk. The primary antibodies and specific dilutions used were as follows: mouse anti-GSK3 α/β (1:2,000; Santa Cruz Biotechnology), rabbit anti-RhoA (1:1,000; Cell Signaling Technology), mouse anti-GAPDH (1:40,000; HyTec). Horseradish peroxidase (HRP) conjugates of sheep anti-mouse (1:10,000; Abcam) and goat anti-rabbit (1:1,000; Thermo Fisher Scientific) were used as the secondary antibodies for visualizing proteins using WesternBright Quantum HRP substrate (Advansta). Protein band signals were detected in a ChemiDoc XRS+ documentation system (Bio-Rad) and quantified using the ImageLab software (Bio-Rad). The protein lane density was normalized to the GAPDH loading control, and the percentage of inhibition was calculated as a relative value to the control sample.

Immuno-cytochemistry and Histochemistry

The distribution and cellular uptake of Cy5-AONs were assessed by immunofluorescence in DRG and spinal cord cryosections. For DRG explants: upon fixation with 4% (w/v) PFA for 15 min, whole DRG explants were pulled out from fibrin gels and were frozen in OCT embedding medium (Thermo Fisher Scientific). Serial cryosections (16 μm thick) were made through the entire DRG explant, mounted in gelatin-coated slides and air dried before staining. The DRG middle sections were selected for β-III tubulin staining. Immunocytochemistry was performed as follows: DRG sections were permeabilized with 0.2% (v/v) Triton X-100 (Sigma-Aldrich) in PBS for 10 min, incubated in 5% (v/v) normal goat serum (NGS) (Sigma-Aldrich) blocking solution in 0.05% (v/v) Tween-20 (Sigma-Aldrich) in PBS for 1 hr, stained overnight with rabbit polyclonal β-III tubulin antibody (1:500, Abcam) at 4°C, and finally incubated with goat anti-rabbit Alexa Fluor 488 (1:500, Molecular Probes) for 1 hr in 1% (v/v) NGS solution. Nuclei were counterstained with DAPI for 10 min (0.1 μg/mL, GIBCO). Images were acquired with Leica TCS SP2 or SP5 confocal microscopes (Leica Microsystems, Nussloch, Germany) with 20×/0.7 oil-immersion objective lenses. Maximum projections were obtained using the ImageJ software (v.2.0.0-rc-44/1.50e). For spinal cords: the spinal cord was removed from perfused animals and post-fixed 24 hr in the same fixative, after which it was stored in 30% (w/v) sucrose in PBS at 4°C or −20°C until use. The spinal cord tissues were then embedded in OCT medium, frozen, and sectioned in 16-μm-thick longitudinal (sagittal plane) sections in a cryostat. Cryosections were used for histology with H&E staining, as well as immunohistochemistry (IHC). IHC was performed as follows: slides were first incubated 5 min with 0.1% (w/v) sodium borohydride in Tris-EDTA (pH 9) to block free aldehydes, followed by a 15-min incubation in 50 mM NH_4Cl in PBS. Samples were then blocked in 5% NGS with 0.3% Triton X-100 in PBS for 1 hr. Antibodies used for subsequent staining were as follows: monoclonal rabbit anti-β-III tubulin (1:500, Covance); rabbit anti-GFAP (1:400, Dako); and rabbit anti-IBA1 (1:500, Dako). Goat anti-rabbit Alexa Fluor 488 (1:1,000, Thermo Fisher Scientific) was used as secondary antibody. Nuclei were counterstained with Hoechst 33342 (Thermo Fisher Scientific) (1:10,000 dilution in 1× PBS from a solution at 10 mg/mL) for 10 min.

Images were captured using an inverted microscope (Axiovert 200M, Zeiss) or laser scanning confocal microscope (Leica TCS SP5).

Statistical Analysis

GraphPad Prism 6 was used for graphical representation of results and statistical analysis. Tests used for calculation of statistical significance are described in the corresponding figures. Results with $p < 0.05$ were considered statistically significant.

SUPPLEMENTAL INFORMATION

Supplemental Information includes four figures and can be found with this article online at https://doi.org/10.1016/j.omtn.2018.03.009.

AUTHOR CONTRIBUTIONS

P.M.D.M designed experiments, was involved in the overall experimental work, and wrote the manuscript. A.R.F., M.T., and E.D.C. were involved in the *in vitro* and *in vivo* experimentation and manuscript preparation. D.S. and M.T.R were involved in *in vivo* experimentation and manuscript preparation. U.T. was involved in AON design and synthesized AONs. M.M.S. contributed to study design and contributed to manuscript preparation. I.F.A. contributed to study design, provided assistance with hydrogel design, and contributed to manuscript preparation. J.W. contributed to LNA-AON design, synthesized LNA-AONs, and contributed to manuscript preparation. A.P.P provided leadership, conceived the project, designed experiments, and prepared and reviewed the manuscript.

ACKNOWLEDGMENTS

This work was supported by Fundação para a Ciência e a Tecnologia (FCT, Portugal) in the framework of the Harvard-Portugal Medical School Program (HMSP-ICT/0020/2010); Project NORTE-01-0145-FEDER-000008, supported by the Norte Portugal Regional Operational Programme (NORTE 2020), under the PORTUGAL 2020 Partnership Agreement, through the European Regional Development Fund (ERDF); Fundo Europeu de Desenvolvimento Regional funds through COMPETE 2020 - Operational Program for Competitiveness and Internationalization (POCI), Portugal 2020; by Portuguese funds through FCT/Ministério da Ciência, Tecnologia e Ensino Superior in the framework of the project "Institute for Research and Innovation in Health Sciences" (POCI-01-0145-FEDER-007274); Marie

Curie Actions of the European Community's 7th Framework Program (PIEF-GA-2011-300485 to P.M.D.M.); Santa Casa da Misericordia de Lisboa – Prémio Neurociências Mello e Castro, and FCT fellowship SFRH/BPD/108738/2015 (to P.M.D.M). Funding for open access charge: Project NORTE-01-0145-FEDER-000012, financed by Norte Portugal Regional Operational Programme (NORTE 2020), under the PORTUGAL 2020 Partnership Agreement, through the ERDF.

We would like to acknowledge the support from Paula Magalhães and Tânia Meireles from the i3S Cell Culture and Genotyping Core Facility in real-time PCR experiments.

REFERENCES

1. Pêgo, A.P., Kubinova, S., Cizkova, D., Vanicky, I., Mar, F.M., Sousa, M.M., and Sykova, E. (2012). Regenerative medicine for the treatment of spinal cord injury: more than just promises? J. Cell. Mol. Med. *16*, 2564–2582.
2. Brazda, N., and Müller, H.W. (2009). Pharmacological modification of the extracellular matrix to promote regeneration of the injured brain and spinal cord. Prog. Brain Res. *175*, 269–281.
3. Yiu, G., and He, Z. (2006). Glial inhibition of CNS axon regeneration. Nat. Rev. Neurosci. *7*, 617–627.
4. Filbin, M.T. (2003). Myelin-associated inhibitors of axonal regeneration in the adult mammalian CNS. Nat. Rev. Neurosci. *4*, 703–713.
5. Wang, X., Cao, K., Sun, X., Chen, Y., Duan, Z., Sun, L., Guo, L., Bai, P., Sun, D., Fan, J., et al. (2015). Macrophages in spinal cord injury: phenotypic and functional change from exposure to myelin debris. Glia *63*, 635–651.
6. Tohda, C., and Kuboyama, T. (2011). Current and future therapeutic strategies for functional repair of spinal cord injury. Pharmacol. Ther. *132*, 57–71.
7. Ramer, L.M., Ramer, M.S., and Bradbury, E.J. (2014). Restoring function after spinal cord injury: towards clinical translation of experimental strategies. Lancet Neurol. *13*, 1241–1256.
8. Hagedorn, P.H., Persson, R., Funder, E.D., Albæk, N., Diemer, S.L., Hansen, D.J., Møller, M.R., Papargyri, N., Christiansen, H., Hansen, B.R., et al. (2018). Locked nucleic acid: modality, diversity, and drug discovery. Drug Discov. Today *23*, 101–114.
9. Bennett, C.F., and Swayze, E.E. (2010). RNA targeting therapeutics: molecular mechanisms of antisense oligonucleotides as a therapeutic platform. Annu. Rev. Pharmacol. Toxicol. *50*, 259–293.
10. Saonere, J.A. Antisense therapy, a magic bullet for the treatment of various diseases: Present and future prospects. J. Med. Genet. Genomics *3*, 77–83.
11. Butler, M., Hayes, C.S., Chappell, A., Murray, S.F., Yaksh, T.L., and Hua, X.Y. (2005). Spinal distribution and metabolism of 2′-O-(2-methoxyethyl)-modified oligonucleotides after intrathecal administration in rats. Neuroscience *131*, 705–715.
12. Smith, R.A., Miller, T.M., Yamanaka, K., Monia, B.P., Condon, T.P., Hung, G., Lobsiger, C.S., Ward, C.M., McAlonis-Downes, M., Wei, H., et al. (2006). Antisense oligonucleotide therapy for neurodegenerative disease. J. Clin. Invest. *116*, 2290–2296.
13. Rigo, F., Chun, S.J., Norris, D.A., Hung, G., Lee, S., Matson, J., Fey, R.A., Gaus, H., Hua, Y., Grundy, J.S., et al. (2014). Pharmacology of a central nervous system delivered 2′-O-methoxyethyl-modified survival of motor neuron splicing oligonucleotide in mice and nonhuman primates. J. Pharmacol. Exp. Ther. *350*, 46–55.
14. Koller, E., Vincent, T.M., Chappell, A., De, S., Manoharan, M., and Bennett, C.F. (2011). Mechanisms of single-stranded phosphorothioate modified antisense oligonucleotide accumulation in hepatocytes. Nucleic Acids Res. *39*, 4795–4807.
15. Castanotto, D., Lin, M., Kowolik, C., Wang, L., Ren, X.-Q., Soifer, H.S., Koch, T., Hansen, B.R., Oerum, H., Armstrong, B., et al. (2015). A cytoplasmic pathway for gapmer antisense oligonucleotide-mediated gene silencing in mammalian cells. Nucleic Acids Res. *43*, 9350–9361.
16. Fazil, M.H.U.T., Ong, S.T., Chalasani, M.L.S., Low, J.H., Kizhakeyil, A., Mamidi, A., Lim, C.F., Wright, G.D., Lakshminarayanan, R., Kelleher, D., and Verma, N.K. (2016). GapmeR cellular internalization by macropinocytosis induces sequence-specific gene silencing in human primary T-cells. Sci. Rep. *6*, 37721.
17. Kordasiewicz, H.B., Stanek, L.M., Wancewicz, E.V., Mazur, C., McAlonis, M.M., Pytel, K.A., Artates, J.W., Weiss, A., Cheng, S.H., Shihabuddin, L.S., et al. (2012). Sustained therapeutic reversal of Huntington's disease by transient repression of huntingtin synthesis. Neuron *74*, 1031–1044.
18. Miller, T.M., Pestronk, A., David, W., Rothstein, J., Simpson, E., Appel, S.H., Andres, P.L., Mahoney, K., Allred, P., Alexander, K., et al. (2013). An antisense oligonucleotide against SOD1 delivered intrathecally for patients with SOD1 familial amyotrophic lateral sclerosis: a phase 1, randomised, first-in-man study. Lancet Neurol. *12*, 435–442.
19. Lei, Y., Rahim, M., Ng, Q., and Segura, T. (2011). Hyaluronic acid and fibrin hydrogels with concentrated DNA/PEI polyplexes for local gene delivery. J. Control. Release *153*, 255–261.
20. Kowalczewski, C.J., and Saul, J.M. (2015). Surface-mediated delivery of siRNA from fibrin hydrogels for knockdown of the BMP-2 binding antagonist noggin. Acta Biomater. *25*, 109–120.
21. Pannier, A.K., and Segura, T. (2013). Surface- and hydrogel-mediated delivery of nucleic acid nanoparticles. Methods Mol. Biol. *948*, 149–169.
22. Petter-Puchner, A.H., Froetscher, W., Krametter-Froetscher, R., Lorinson, D., Redl, H., and van Griensven, M. (2007). The long-term neurocompatibility of human fibrin sealant and equine collagen as biomatrices in experimental spinal cord injury. Exp. Toxicol. Pathol. *58*, 237–245.
23. King, V.R., Alovskaya, A., Wei, D.Y.T., Brown, R.A., and Priestley, J.V. (2010). The use of injectable forms of fibrin and fibronectin to support axonal ingrowth after spinal cord injury. Biomaterials *31*, 4447–4456.
24. Johnson, P.J., Parker, S.R., and Sakiyama-Elbert, S.E. (2010). Fibrin-based tissue engineering scaffolds enhance neural fiber sprouting and delay the accumulation of reactive astrocytes at the lesion in a subacute model of spinal cord injury. J. Biomed. Mater. Res. A *92*, 152–163.
25. Sharp, K.G., Dickson, A.R., Marchenko, S.A., Yee, K.M., Emery, P.N., Laidmåe, I., Uibo, R., Sawyer, E.S., Steward, O., and Flanagan, L.A. (2012). Salmon fibrin treatment of spinal cord injury promotes functional recovery and density of serotonergic innervation. Exp. Neurol. *235*, 345–356.
26. Lundin, K.E., Højland, T., Hansen, B.R., Persson, R., Bramsen, J.B., Kjems, J., Koch, T., Wengel, J., and Smith, C.I. (2013). Biological activity and biotechnological aspects of locked nucleic acids. Adv. Genet. *82*, 47–107.
27. Veedu, R.N., and Wengel, J. (2009). Locked nucleic acid as a novel class of therapeutic agents. RNA Biol. *6*, 321–323.
28. Moreno, P.M.D., Geny, S., Pabon, Y.V., Bergquist, H., Zaghloul, E.M., Rocha, C.S.J., Oprea, I.I., Bestas, B., Andaloussi, S.E., Jørgensen, P.T., et al. (2013). Development of bis-locked nucleic acid (bisLNA) oligonucleotides for efficient invasion of supercoiled duplex DNA. Nucleic Acids Res. *41*, 3257–3273.
29. Stein, C.A., Hansen, J.B., Lai, J., Wu, S., Voskresenskiy, A., Høg, A., Worm, J., Hedtjärn, M., Souleimanian, N., Miller, P., et al. (2010). Efficient gene silencing by delivery of locked nucleic acid antisense oligonucleotides, unassisted by transfection reagents. Nucleic Acids Res. *38*, e3.
30. Wahlestedt, C., Salmi, P., Good, L., Kela, J., Johnsson, T., Hökfelt, T., Broberger, C., Porreca, F., Lai, J., Ren, K., et al. (2000). Potent and nontoxic antisense oligonucleotides containing locked nucleic acids. Proc. Natl. Acad. Sci. USA *97*, 5633–5638.
31. McKerracher, L., and Higuchi, H. (2006). Targeting Rho to stimulate repair after spinal cord injury. J. Neurotrauma *23*, 309–317.
32. Fehlings, M.G., Theodore, N., Harrop, J., Maurais, G., Kuntz, C., Shaffrey, C.I., Kwon, B.K., Chapman, J., Yee, A., Tighe, A., and McKerracher, L. (2011). A phase I/IIa clinical trial of a recombinant Rho protein antagonist in acute spinal cord injury. J. Neurotrauma *28*, 787–796.
33. Xing, B., Li, H., Wang, H., Mukhopadhyay, D., Fisher, D., Gilpin, C.J., and Li, S. (2011). RhoA-inhibiting NSAIDs promote axonal myelination after spinal cord injury. Exp. Neurol. *231*, 247–260.
34. Seira, O., Gavín, R., Gil, V., Llorens, F., Rangel, A., Soriano, E., and del Río, J.A. (2010). Neurites regrowth of cortical neurons by GSK3beta inhibition independently of Nogo receptor 1. J. Neurochem. *113*, 1644–1658.

35. Hur, E.-M., Saijilafu, Lee, B.D., Kim, S.J., Xu, W.L., and Zhou, F.Q. (2011). GSK3 controls axon growth via CLASP-mediated regulation of growth cone microtubules. Genes Dev. *25*, 1968–1981.

36. Liz, M.A., Mar, F.M., Santos, T.E., Pimentel, H.I., Marques, A.M., Morgado, M.M., Vieira, S., Sousa, V.F., Pemble, H., Wittmann, T., et al. (2014). Neuronal deletion of GSK3β increases microtubule speed in the growth cone and enhances axon regeneration via CRMP-2 and independently of MAP1B and CLASP2. BMC Biol. *12*, 47.

37. Lord-Fontaine, S., Yang, F., Diep, Q., Dergham, P., Munzer, S., Tremblay, P., and McKerracher, L. (2008). Local inhibition of Rho signaling by cell-permeable recombinant protein BA-210 prevents secondary damage and promotes functional recovery following acute spinal cord injury. J. Neurotrauma *25*, 1309–1322.

38. Cuzzocrea, S., Genovese, T., Mazzon, E., Crisafulli, C., Di Paola, R., Muià, C., Collin, M., Esposito, E., Bramanti, P., and Thiemermann, C. (2006). Glycogen synthase kinase-3 beta inhibition reduces secondary damage in experimental spinal cord trauma. J. Pharmacol. Exp. Ther. *318*, 79–89.

39. Gerin, C.G., Madueke, I.C., Perkins, T., Hill, S., Smith, K., Haley, B., Allen, S.A., Garcia, R.P., Paunesku, T., and Woloschak, G. (2011). Combination strategies for repair, plasticity, and regeneration using regulation of gene expression during the chronic phase after spinal cord injury. Synapse *65*, 1255–1281.

40. Madden, T. (2015). The BLAST sequence analysis tool. In The NCBI Handbook [Internet], J. McEntyre and J. Ostell, eds. (National Center for Biotechnology Information). https://doi.org/10.1016/s0958-1669(98)80126-2.

41. Kurreck, J., Wyszko, E., Gillen, C., and Erdmann, V.A. (2002). Design of antisense oligonucleotides stabilized by locked nucleic acids. Nucleic Acids Res. *30*, 1911–1918.

42. Man, A.J., Davis, H.E., Itoh, A., Leach, J.K., and Bannerman, P. (2011). Neurite outgrowth in fibrin gels is regulated by substrate stiffness. Tissue Eng. Part A *17*, 2931–2942.

43. Cheriyan, T., Ryan, D.J., Weinreb, J.H., Cheriyan, J., Paul, J.C., Lafage, V., Kirsch, T., and Errico, T.J. (2014). Spinal cord injury models: a review. Spinal Cord *52*, 588–595.

44. Pires, L.R., Rocha, D.N., Ambrosio, L., and Pêgo, A.P. (2015). The role of the surface on microglia function: implications for central nervous system tissue engineering. J. R. Soc. Interface *12*, 20141224.

45. Rocha, D.N., Brites, P., Fonseca, C., and Pêgo, A.P. (2014). Poly(trimethylene carbonate-co-ε-caprolactone) promotes axonal growth. PLoS ONE *9*, e88593.

46. Vickers, T.A., Freier, S.M., Bui, H.-H., Watt, A., and Crooke, S.T. (2014). Targeting of repeated sequences unique to a gene results in significant increases in antisense oligonucleotide potency. PLoS ONE *9*, e110615.

47. Kasuya, T., Hori, S., Watanabe, A., Nakajima, M., Gahara, Y., Rokushima, M., Yanagimoto, T., and Kugimiya, A. (2016). Ribonuclease H1-dependent hepatotoxicity caused by locked nucleic acid-modified gapmer antisense oligonucleotides. Sci. Rep. *6*, 30377.

48. Burel, S.A., Hart, C.E., Cauntay, P., Hsiao, J., Machemer, T., Katz, M., Watt, A., Bui, H.H., Younis, H., Sabripour, M., et al. (2016). Hepatotoxicity of high affinity gapmer antisense oligonucleotides is mediated by RNase H1 dependent promiscuous reduction of very long pre-mRNA transcripts. Nucleic Acids Res. *44*, 2093–2109.

49. DeVos, S.L., and Miller, T.M. (2013). Antisense oligonucleotides: treating neurodegeneration at the level of RNA. Neurotherapeutics *10*, 486–497.

50. Evers, M.M., Toonen, L.J.A., and van Roon-Mom, W.M.C. (2015). Antisense oligonucleotides in therapy for neurodegenerative disorders. Adv. Drug Deliv. Rev. *87*, 90–103.

51. Bestas, B., Moreno, P.M.D., Blomberg, K.E.M., Mohammad, D.K., Saleh, A.F., Sutlu, T., Nordin, J.Z., Guterstam, P., Gustafsson, M.O., Kharazi, S., et al. (2014). Splice-correcting oligonucleotides restore BTK function in X-linked agammaglobulinemia model. J. Clin. Invest. *124*, 4067–4081.

52. Moreno, P.M.D., and Pêgo, A.P. (2014). Therapeutic antisense oligonucleotides against cancer: hurdling to the clinic. Front Chem. *2*, 87.

53. Geary, R.S., Crooke, R., Bhanot, S., and Singleton, W. (2014). Antisense therapies for cardiovascular/ metabolic diseases. Drug Discov. Today Ther. Strateg. *10*, e165–e170.

54. Rocha, C.S.J., Wiklander, O.P.B., Larsson, L., Moreno, P.M.D., Parini, P., Lundin, K.E., and Smith, C.I. (2015). RNA therapeutics inactivate PCSK9 by inducing a unique intracellular retention form. J. Mol. Cell. Cardiol. *82*, 186–193.

55. Grijalvo, S., Aviñó, A., and Eritja, R. (2014). Oligonucleotide delivery: a patent review (2010 - 2013). Expert Opin. Ther. Pat. *24*, 801–819.

56. Aartsma-Rus, A. (2016). New momentum for the field of oligonucleotide therapeutics. Mol. Ther. *24*, 193–194.

57. Afshari, F.T., Kappagantula, S., and Fawcett, J.W. (2009). Extrinsic and intrinsic factors controlling axonal regeneration after spinal cord injury. Expert Rev. Mol. Med. *11*, e37.

58. Figueroa, J.D., Benton, R.L., Velazquez, I., Torrado, A.I., Ortiz, C.M., Hernandez, C.M., Diaz, J.J., Magnuson, D.S., Whittemore, S.R., and Miranda, J.D. (2006). Inhibition of EphA7 up-regulation after spinal cord injury reduces apoptosis and promotes locomotor recovery. J. Neurosci. Res. *84*, 1438–1451.

59. Simard, J.M., Woo, S.K., Norenberg, M.D., Tosun, C., Chen, Z., Ivanova, S., Tsymbalyuk, O., Bryan, J., Landsman, D., and Gerzanich, V. (2010). Brief suppression of Abcc8 prevents autodestruction of spinal cord after trauma. Sci. Transl. Med. *2*, 28ra29.

60. Cheng, H., Cao, Y., and Olson, L. (1996). Spinal cord repair in adult paraplegic rats: partial restoration of hind limb function. Science *273*, 510–513.

61. Spicer, P.P., and Mikos, A.G. (2010). Fibrin glue as a drug delivery system. J. Control. Release *148*, 49–55.

62. Taylor, S.J., McDonald, J.W., 3rd, and Sakiyama-Elbert, S.E. (2004). Controlled release of neurotrophin-3 from fibrin gels for spinal cord injury. J. Control. Release *98*, 281–294.

63. Walthers, C.M., and Seidlits, S.K. (2015). Gene delivery strategies to promote spinal cord repair. Biomark. Insights *10* (*Suppl 1*), 11–29.

64. Straarup, E.M., Fisker, N., Hedtjärn, M., Lindholm, M.W., Rosenbohm, C., Aarup, V., Hansen, H.F., Ørum, H., Hansen, J.B., and Koch, T. (2010). Short locked nucleic acid antisense oligonucleotides potently reduce apolipoprotein B mRNA and serum cholesterol in mice and non-human primates. Nucleic Acids Res. *38*, 7100–7111.

65. Sheehan, J.P., and Lan, H.C. (1998). Phosphorothioate oligonucleotides inhibit the intrinsic tenase complex. Blood *92*, 1617–1625.

66. Yakovlev, S., Gorlatov, S., Ingham, K., and Medved, L. (2003). Interaction of fibrin (ogen) with heparin: further characterization and localization of the heparin-binding site. Biochemistry *42*, 7709–7716.

67. Juliano, R., Alam, M.R., Dixit, V., and Kang, H. (2008). Mechanisms and strategies for effective delivery of antisense and siRNA oligonucleotides. Nucleic Acids Res. *36*, 4158–4171.

68. Goodman, T.T., Ng, C.P., and Pun, S.H. (2008). 3-D tissue culture systems for the evaluation and optimization of nanoparticle-based drug carriers. Bioconjug. Chem. *19*, 1951–1959.

69. Stanton, R., Sciabola, S., Salatto, C., Weng, Y., Moshinsky, D., Little, J., Walters, E., Kreeger, J., DiMattia, D., Chen, T., et al. (2012). Chemical modification study of antisense gapmers. Nucleic Acid Ther. *22*, 344–359.

70. Dubreuil, C.I., Winton, M.J., and McKerracher, L. (2003). Rho activation patterns after spinal cord injury and the role of activated Rho in apoptosis in the central nervous system. J. Cell Biol. *162*, 233–243.

71. Yuskaitis, C.J., and Jope, R.S. (2009). Glycogen synthase kinase-3 regulates microglial migration, inflammation, and inflammation-induced neurotoxicity. Cell. Signal. *21*, 264–273.

72. Kamola, P.J., Kitson, J.D.A., Turner, G., Maratou, K., Eriksson, S., Panjwani, A., Warnock, L.C., Douillard Guilloux, G.A., Moores, K., Koppe, E.L., et al. (2015). In silico and in vitro evaluation of exonic and intronic off-target effects form a critical element of therapeutic ASO gapmer optimization. Nucleic Acids Res. *43*, 8638–8650.

73. Hagedorn, P.H., Hansen, B.R., Koch, T., and Lindow, M. (2017). Managing the sequence-specificity of antisense oligonucleotides in drug discovery. Nucleic Acids Res. *45*, 2262–2282.

74. Campbell, R.A., Overmyer, K.A., Bagnell, C.R., and Wolberg, A.S. (2008). Cellular procoagulant activity dictates clot structure and stability as a function of distance from the cell surface. Arterioscler. Thromb. Vasc. Biol. *28*, 2247–2254.

75. Pires, L.R., Lopes, C.D.F., Salvador, D., Rocha, D.N., and Pêgo, A.P. (2017). Ibuprofen-loaded fibrous patches-taming inhibition at the spinal cord injury site. J. Mater. Sci. Mater. Med. *28*, 157.

76. Sierakowska, H., Sambade, M.J., Agrawal, S., and Kole, R. (1996). Repair of thalassemic human beta-globin mRNA in mammalian cells by antisense oligonucleotides. Proc. Natl. Acad. Sci. USA *93*, 12840–12844.